Toxoplasma gondii requires its plant-like heme biosynthesis pathway for infection.

Amy Bergmann[#1], Katherine Floyd[#1], Melanie Key[1], Carly Dameron[1], Kerrick C. Rees[2], Daniel C. Whitehead[2], Iqbal Hamza[3,4], Zhicheng Dou[*1]

1. Department of Biological Sciences, Clemson University, Clemson, South Carolina, USA 29634
2. Department of Chemistry, Clemson University, Clemson, South Carolina, USA 29634
3. Department of Animal and Avian Sciences, University of Maryland, College Park, Maryland, USA 20742
4. Department of Cell Biology and Molecular Genetics, University of Maryland, College Park, Maryland, USA 20742

#, These authors contributed equally to this work; *, corresponding author.

Corresponding author: Zhicheng Dou (zdou@clemson.edu)

Short title: Heme metabolism in *Toxoplasma gondii*

Heme, an iron-enclosed organic ring, is essential for virtually all living organisms by serving as a prosthetic group in proteins that function in diverse cellular activities ranging from diatomic gas transport and detection to mitochondrial respiration to detoxification. Cellular heme levels in microbial pathogens can be a composite of endogenous *de novo* synthesis or exogenous uptake of heme or heme synthesis intermediates[1,2]. Intracellular pathogenic microbes switch routes for heme supply when heme availability in their replicative environment fluctuates through infections[2]. Here, we show that the *Toxoplasma gondii*, an obligate intracellular human pathogen, encodes a functional heme biosynthesis pathway. A chloroplast-derived organelle, termed apicoplast, is involved in the heme production. Genetic and chemical manipulation revealed that *de novo* heme production is essential for *T. gondii* intracellular growth and pathogenesis. Surprisingly, the

herbicide oxadiazon significantly impaired *Toxoplasma* growth, consistent with phylogenetic analyses that show *T. gondii* protoporphyrinogen oxidase is more closely related to plants than mammals. We further improve upon this inhibition by 15- to 25-fold with two oxadiazon derivatives, providing therapeutic proof that *Toxoplasma* heme biosynthesis is a druggable target. As *T. gondii* has been used to model other apicomplexan parasites[3], our study underscores the utility of targeting heme biosynthesis in other pathogenic apicomplexans.

Human protozoan pathogens share some common nutrient metabolism pathways with their counterparts in the host but show distinct features. Apicomplexan parasites, including *Toxoplasma gondii* and *Plasmodium spp.,* encode a complete *de novo* heme biosynthesis pathway in their genomes[2] (Fig. 1a). In *Toxoplasma*, a previous study of ectopic overexpression of all 8 heme biosynthetic proteins revealed that these enzymes are delivered to three subcellular locations[4], including the mitochondrion, cytoplasm, and apicoplast. The apicoplast is a remnant chloroplast and specifically exists in apicomplexan parasites. Moreover, the second enzyme residing within the parasite's heme biosynthesis pathway, *Toxoplasma* porphobilinogen synthase (TgPBGS), was expressed in an active recombinant form[5,6]. These previous findings revealed that the heme biosynthetic enzymes in *Toxoplasma* carry targeting signals for their subcellular localization, and one of these enzymes, TgPBGS, is enzymatically functional. However, it still remains unknown whether the entire pathway is active for heme production during *Toxoplasma* infections, and this pathway plays a critical role in *Toxoplasma* infection.

As an intracellular parasite, *Toxoplasma* utilizes the host plasma membrane to create its own membrane-bound compartment for intracellular replication, termed the parasitophorous vacuole (PV)[7]. The PV membrane (PVM) is permeable for small solutes. Studies have demonstrated that putative nutrient pores exist on the PVM that allows small substances with molecular weights less than ~1,300 Da to diffuse into the PV[8]. A recent study revealed that the parasites use two dense granule proteins, TgGRA17 and TgGRA23, to form a pore structure on the PVM, which allows small molecules to enter the PV from host cytoplasm[9]. One such small molecule is heme, a prosthetic group found in a number of essential proteins, leading to the hypothesis that parasites can hijack the host's heme or heme synthesis intermediates (Fig.

55 1a). Since *Toxoplasma* can ingest and digest host proteins to support its growth[10], *Toxoplasma* may
56 acquire heme through liberating it from the digestion of host's hemoproteins. Collectively, both the
57 parasite's *de novo* heme production and/or heme acquisition from the host may contribute to parasite
58 replication and infection. Interestingly, the *de novo* heme production is dispensable in the blood-stage
59 infection of *Plasmodium falciparum*[11], a malaria-causing agent, but is required for its liver-stage
60 infection[12,13], suggesting that intracellular pathogens could switch their metabolism for heme needs due to
61 their access to exogenous heme availability.

62 To test whether all 8 genes residing within *Toxoplasma*'s *de novo* heme biosynthesis pathway are
63 expressed in the acute infection stage, we endogenously inserted epitope tags at their C-termini (Fig. S1a).
64 Immunoblotting revealed their active expression during acute toxoplasmosis (Fig. S1c). In addition,
65 fluorescence localization experiments confirmed that *Toxoplasma* distributes its heme biosynthesis in the
66 mitochondrion, cytoplasm, and apicoplast (Fig. 1b). Overall, our findings revealed that *Toxoplasma*
67 maintains *de novo* heme biosynthetic components during acute infection.

68 Given the possibility that *Toxoplasma* could rely on its *de novo* heme production or scavenge heme or
69 its intermediates from the host to support infection, we deleted 5-aminolevulinic acid (ALA) synthase
70 (*TgALAS*, TGGT1_258690), the first enzyme in the pathway, in a NanoLuc luciferase-expressing wildtype
71 (WT::*NLuc*) *Toxoplasma*. Disruption of *TgALAS* will specifically block the parasite's *de novo* heme
72 biosynthesis but maintain the downstream pathway intact for possible utilization of host-derived heme
73 intermediates (Fig. 1a). Generation of Δ*alas* in standard growth medium was unsuccessful until the medium
74 was supplemented with 300 μM ALA, the product of TgALAS, suggesting that the *de novo* heme production
75 is essential for parasite infection. To test this, we evaluated the replication of the resulting Δ*alas::NLuc*
76 mutant after it was starved in ALA-free medium for 144 h. The starved Δ*alas*::*NLuc* exhibited severe
77 replication defects compared to WT::*NLuc* and Δ*alasALAS*::*NLuc* (a *TgALAS* complementation strain), and
78 also grew more slowly in the medium lacking ALA during replication relative to the starved Δ*alas*::*NLuc*
79 replicated in the ALA-containing medium (Fig. 2a). Additionally, the Δ*alas*::*NLuc* parasites showed severe
80 growth defects by using a luciferase-based growth assay (Fig. S5a). To further assess the viability of the
81 Δ*alas*::*NLuc* parasites in the absence of ALA, we monitored its growth over 10 days post-ALA starvation.

82 The Δ*alas*::*NLuc* mutant gradually slowed down its replication, but remained viable (Fig. 2b), suggesting
83 that the parasites may incorporate a residual level of heme and/or heme synthesis intermediates from the
84 host. To test the role of TgALAS in parasite acute virulence, we subcutaneously injected the Δ*alas*::*NLuc*
85 mutant along with WT::*NLuc* and Δ*alasALAS*::*NLuc* strains into CD-1 mice and did not observe mortality
86 in the mice infected with the Δ*alas* strain, even when its inocula were 10^3- and 10^4-fold higher than that
87 required for WT parasites to establish a lethal infection (Fig. 2c). As expected, the infections derived from
88 WT::*NLuc* and Δ*alasALAS*::*NLuc* strains were lethal at 10-12 days post-infection (Fig. 2c). That surviving
89 mice were infected was confirmed by seroconversion and their resistance to subsequent challenge with
90 WT parasites.

91 To further confirm that the heme biosynthesis pathway is crucial in *Toxoplasma*, we attempted to ablate
92 the ferrochelatase (*TgFECH*, TGGT1_258650), which catalyzes the last step in heme production. We
93 detected the correct integration of the drug resistance cassette into the *TgFECH* locus (Fig. S2d) but were
94 unable to generate the straight Δ*fech* knockout, even upon supplementing the medium with 10 μM heme.
95 Alternatively, we generated a *TgFECH* knockdown strain using a tetracycline-controlled TET-OFF system.
96 To recognize the targeted *TgFECH*, we endogenously tagged its C-terminus with a 3xmyc epitope before
97 replacing its cognate promoter with a T7S4 promoter, a hybrid of the promoter of *Toxoplasma SAG4*
98 (surface antigen 4) gene and the ATc-responsive promoter (Fig. S3a). The expression of *TgFECH* in the
99 resulting knockdown strain, named T7S4-TgFECH-3xmyc, was below the limit of detection after 144-h
100 treatment of ATc (Fig. 2d), and the *TgFECH*-deficient mutant showed a drastic replication defect (Fig. 2e).
101 Interestingly, if the *TgFECH* repression was halted during the replication assay by removing ATc, T7S4-
102 TgFECH-3xmyc parasites significantly increased their replication rate compared to those grown in ATc-
103 containing medium, validating the key role of the *de novo* heme biosynthesis in parasite intracellular growth
104 (Fig. 2e). Additionally, we individually deleted coproporphyrinogen oxidase (*TgCPOX*, TGGT1_223020)
105 and protoporphyrinogen oxidase (*TgPPO*, TGGT1_272490) within the pathway. The *TgCPOX*- and
106 *TgPPO*-lacking mutants (Δ*cpox* and Δ*ppo*) displayed approximately 75% and 50% reduction in replication,
107 respectively, compared to WT (Fig. 2f-g). A luciferase-based assay also confirmed that both knockout
108 mutants showed severe growth defects compared to WT parasites (Fig. S5b-c). The deletion of *TgCPOX*

109 or *TgPPO* also resulted in the complete loss of acute virulence in *Toxoplasma* (Fig. 2h-i). Given that both
110 TgCPOX and TgPPO are oxidases, such oxidation reactions can occur even without enzymatic catalysis,
111 albeit at lower reaction rates, which could explain why the growth defects of both knockouts were not as
112 severe as that of *TgALAS* and *TgFECH*-deficient parasites. These findings are also consistent with *S.*
113 *cerevisiae* wherein PPO is the only non-essential protein within its heme biosynthesis pathway[14]. In
114 addition, *Toxoplasma* encodes an oxygen-independent coproporphyrinogen dehydrogenase (*TgCPDH*,
115 TGGT1_288640), which may also help bypass the reaction catalyzed by TgCPOX to sustain partial *de*
116 *novo* heme production in the parasites, albeit possibly at a lower level. Collectively, the systematic
117 phenotypic characterization of a series of mutants lacking a functional *de novo* heme production in
118 *Toxoplasma* established its crucial importance in parasite growth and pathogenesis. Although *Toxoplasma*
119 may acquire heme or its intermediates from the host via a salvage pathway, it is not sufficient for supporting
120 normal parasite growth and acute virulence.

121 To determine that the parasite's *de novo* heme biosynthesis pathway is active, we complemented *S.*
122 *cerevisiae* heme-deficient mutants lacking *ALAS*, *CPOX*, or *FECH* with the corresponding *Toxoplasma*
123 ortholog genes. The resulting complementation strains had their heme auxotrophy phenotypes restored
124 (Fig. 3a), whereas the strains complemented with the empty vector did not grow on heme-free media.
125 These data, thus, established that TgALAS, TgCPOX, and TgFECH enzymes are functional. Additionally,
126 the total heme abundance in heme biosynthetic gene knockout and knockdown parasites was quantified
127 using a protoporphyrin IX-based fluorescence assay[14]. The total heme abundances in the Δ*cpox* and Δ*ppo*
128 were reduced by approximately 75% and 50%, respectively (Fig. 3b). The heme level in Δ*alas* was nearly
129 50% relative to WT parasites when it was grown in medium supplemented with 300 μM ALA, but fell to
130 approximately 10% when ALA was depleted (Fig. 3b). Similarly, the heme abundance in *TgFECH*
131 knockdown strain was decreased to *ca.*15% compared to its parental strain when the mutant was treated
132 with ATc for 144 h to repress *TgFECH* expression (Fig. 3b). Interestingly, the parasite replication rate was
133 positively correlated to the total heme abundance in the parasites (Fig. 3b).

134 We also evaluated whether the *de novo* heme production within *Toxoplasma* is responsive to chemical
135 interference. Succinylacetone (SA), which inhibits *de novo* heme production by targeting TgPBGS activity,

136 or ALA, which stimulates heme production, were used for chemical interrogation of the pathway (Fig. 1a).
137 Initially, we determined that the concentration of SA that inhibited parasite growth by 50% (IC_{50}) was 665.5
138 μM using a luciferase-based growth assay (Fig. S7). Next, we grew T7S4-TgFECH and its parental strain
139 in the ATc-containing media for 144 h, followed by the addition of SA or ALA for an additional 48 h before
140 heme quantification. The heme levels in parental parasites were increased ~40% by inclusion of ALA and
141 reduced ~70% due to SA treatment (Fig. 3c), compared to DMSO (vehicle control)-treated parasites.
142 However, ALA and SA did not alter heme levels in the ATc-treated T7S4-TgFECH strain (Fig. 3c). We also
143 found that the inclusion of ALA in the medium improved parasite replication when the *de novo* heme
144 biosynthesis pathway was partially restored in the T7S4-TgFECH strain (Fig. 3d). These findings suggest
145 that the parasite's *de novo* heme biosynthesis pathway actively responds to chemical stimuli for heme
146 production and the fluctuation of heme abundance in host cells does not impact heme levels within the
147 parasites. Taken together, these results indicated that *Toxoplasma* possesses an active heme
148 biosynthesis pathway for their heme supply.

149 In plants, protoporphyrinogen oxidase (PPO) is involved in heme and chlorophyll production[15].
150 Chlorophyll is an essential pigment for photosynthesis in plants[16]. When PPO activity is inhibited in plants,
151 the reactant of PPO, protoporphyrinogen IX, leaks into the cytoplasm and is spontaneously oxidized to
152 protoporphyrin IX, which can absorb light to produce highly reactive singlet oxygen that destroys plant cell
153 membranes[17]. Hence, PPO has been widely recognized as a target for herbicide development. A
154 comparison of primary sequences of PPOs from mammals, plants, fungi, protozoans, and bacteria
155 indicates that TgPPO is most closely related to plant orthologs (Fig. S8). Therefore, we evaluated 11
156 commercial herbicidal PPO inhibitors against WT *T. gondii* and identified that the IC_{50} values of 5
157 compounds ranged from ~130 to 650 μM for the inhibition of parasite growth as determined by a luciferase-
158 based growth assay (Fig. S9).

159 Because oxadiazon was the most potent compound identified, and in light of its potential for additional
160 medicinal chemistry optimization, we next evaluated two derivatives of the scaffold by modifying a
161 structural homolog, oxadiargyl, by means of straightforward cycloaddition chemistry (Fig. 4a). Both
162 derivatives had improved potency, with IC_{50} values approximately 15-25-fold lower than oxadiazon (Fig.

163 4b). In addition, we found that the Δ*ppo* parasites were less sensitive to these compounds than either WT
164 or Δ*ppoPPO* strains (Fig. 4b). The differences in growth were not noted when WT or Δ*ppo* parasites were
165 treated with pyrimethamine, a clinical antibiotic prescribed against acute toxoplasmosis by inhibiting folic
166 acid synthesis (Fig. 4b). The Δ*ppoPPO* strain was less sensitive to pyrimethamine treatment because a
167 pyrimethamine resistance cassette had been used to generate the *TgPPO* complementation plasmid.
168 These findings suggest that these compounds were targeting TgPPO. Last, heme abundance in WT
169 parasites treated with oxadiazon and its derivatives was reduced approximately 15-20% post-treatment
170 (Fig. 4c), further supporting the notion that these chemicals targeted the heme biosynthesis pathway in the
171 parasites. Notably, none of the compounds were toxic to human foreskin fibroblasts based on an
172 AlarmarBlue-derived cell viability assay (Fig. S10).

173 Given the unsuccessful attempts to delete *TgFECH* in the medium supplemented with heme, we
174 speculate that *Toxoplasma* is unable to acquire adequate heme from the host to support its intracellular
175 growth due to the lack of heme transporter. Supporting this, homology searches using several identified
176 heme transporters as templates[18,19], failed to identify candidate heme transporters in the *Toxoplasma*
177 genome (ToxoDB database). We also used the Δ*cpox* cell line as a proxy to test whether *Toxoplasma* can
178 incorporate extracellular heme to support intracellular replication. There was no significant difference in
179 Δ*cpox* replication between standard growth medium and the medium supplemented with 10 μM heme (Fig.
180 4d). A Δ*cpox* replication assay between standard growth medium and the medium containing 300 μM ALA
181 was included as a positive control (Fig. 4d) since *Toxoplasma* can incorporate extracellular ALA into its
182 heme biosynthesis pathway as described above (Fig. 3c). A similar observation was seen in the
183 intracellular growth of Δ*cpox* parasites between heme-depleted and heme-enriched media (Fig. S11). In
184 contrast, humans can acquire dietary heme[18] and mammalian cells can acquire extracellular heme via
185 heme transporters[18,19]. Therefore, the host can overcome heme deficiency by heme supplementation
186 during chemical inhibition of heme production, whereas the parasites cannot. These observations
187 supported the concept that chemical interrogation of the parasite's heme biosynthesis is a potential
188 therapeutic strategy for controlling toxoplasmosis.

189 In conclusion, we revealed that *Toxoplasma* parasites harbor an active plant-like heme biosynthesis
190 pathway and principally rely on this pathway to produce heme for their intracellular growth and acute
191 virulence. In addition, the current antibiotics against *Toxoplasma* trigger strong side effects in some groups
192 of patients and have limited efficacy on congenital toxoplasmosis. Thus, an urgent need for new
193 therapeutics exists. Our findings shed light on the potential novel therapeutic targets within the parasite's
194 heme biosynthesis pathway for the clinical management of *Toxoplasma* infections.
195

196 **Materials and Methods**

197 **Host cells and parasite culture**

198 Human foreskin fibroblasts (HFFs) were obtained from the American Type Culture Collection (ATCC,
199 catalog number: SCRC-1041). Tissue cultures were maintained at 37ºC with 5% CO_2 in D10 medium
200 (Dulbecco's Modified Eagle Medium, 4.5 g/L glucose, (VWR) supplemented with 10% Cosmic Calf serum
201 (HycloneTM, GE Healthcare Life Sciences SH30087.03), 10 mM HEPES, additional 2 mM L-glutamine,
202 and 10 mM Pen/Strep as instructed by the vendor's manual. The HFF cells were tested for mycoplasma
203 contamination every month. *Toxoplasma* strain RH∆*ku80*∆*hxg* and TaTi∆*ku80*∆*hxg* were obtained from
204 the Carruthers Lab (Univ of Michigan) and the Striepen Lab (Univ of Pennsylvania), respectively, who
205 originally created these *Toxoplasma* parental strains. All *Toxoplasma* strains were maintained *in vitro* by
206 serial passage on HFFs. The ∆*alas*::*NLuc* strain was kept in the D10 medium supplemented with 300 µM
207 ALA.

208

209 **Generation of transgenic *T. gondii* strains**

210 (1) <u>*Endogenously epitope-tagging the heme biosynthetic genes.*</u> The RH∆*ku80*∆*hxg* strain was used as
211 the parental strain for endogenous gene tagging. The *TgALAS*, *TgALAD*, *TgCPOX*, *TgPPO*, and *TgFECH*
212 were endogenously tagged with a 3xHA epitope at their C-termini by CRISPR-Cas9-mediated double
213 crossover recombination as described previously[20]. The *TgPBGD*, *TgUROS*, and *TgUROD* were
214 endogenously tagged with a 3xmyc tag C-terminally using similar methods as mentioned above. Briefly,
215 the guide RNA selected to target the 3'-end of the coding sequence for individual genes was incorporated
216 into a guide RNA expression construct as described previously[21]. This construct also encodes Cas9 protein
217 that assists the guide RNA in generating a double-stranded break at the end of genes of interest. Fifty
218 base pairs of homologous regions upstream and downstream stop codon were engineered into forward
219 and reverse primers, respectively. By PCR, they flanked at the 5'- and 3'-ends of the epitope tag and a
220 drug resistance cassette, respectively, to create a repair template. The guide RNA/Cas9 expression
221 plasmids and the repair template were co-introduced into the parental strain by electroporation. Through
222 double-crossover homologous recombination, the epitope tag and drug resistance cassette were

223 incorporated after the last codon of individual genes (**Fig. S1a**). The resulting strains expressing epitope-
224 tagged genes were drug selected and cloned out. The primers used for the epitope tagging of individual
225 genes are listed in the **Supplementary Table 3**.
226
227 *(2) Genetic ablation of the heme biosynthetic genes.* A similar CRISPR-Cas9-based gene editing strategy
228 was conducted for the deletion of *TgCPOX* and *TgPPO* in RH∆*ku80*∆*hxg* strain, and the ablation of
229 *TgALAS* in RH∆*ku80*::*NLuc* strain generated in our previous study[20]. Similarly, the 50-bp homologous
230 upstream and downstream DNA sequences of the start and stop codons of the corresponding gene,
231 respectively, were incorporated into primers for amplification of the drug resistance cassette by PCR. In
232 the final PCR product, the homologous regions located at both ends of the target gene facilitated the
233 replacement of the gene of interest with a drug resistance cassette by double crossover recombination.
234 For individual genes, the PCR product was mixed with the corresponding guide RNA used for the
235 endogenous gene tagging and electroporated into RH∆*ku80*∆*hxg* or RH∆*ku80*::*NLuc* strains for knockout
236 mutant generation. The correct clones were drug selected and cloned out as described previously[20]. PCR
237 was used to verify the integration of the drug resistance cassette in the correct locus (**Fig. S2a-b**). The
238 primers used for the deletion of individual genes and the verification of the knockout mutants are listed in
239 the **Supplementary Table 3**.
240
241 *(3) Complementation of the heme-deficient Toxoplasma knockouts.* To restore the gene expression in the
242 corresponding heme-deficient knockout, we PCR-amplified the coding sequences of the individual heme
243 biosynthetic genes from the *Toxoplasma* cDNA library and the corresponding 1kb 5'- and 3'-UTR
244 (untranslated regions) from the *Toxoplasma* genomic DNA. All three PCR products for individual genes
245 were assembled into a plasmid vector carrying the pyrimethamine resistance cassette to create the
246 corresponding complementation constructs. For both *TgPPO* and *TgALAS* complementation constructs, a
247 1kb DNA fragment localized around 6kb upstream region of the start codon of the *TgKU80* gene was
248 included in the complementation construct to facilitate a single insertion of the complemented gene into
249 the genome of the knockout strain to keep its expression similar to its endogenous expression level.

250 Approximately twenty micrograms of complementation plasmids were used for transfection. After
251 stabilization by drug selection, the complementation parasites were cloned out. PCR was used to verify
252 the integration of the introduced exogenous genes into the parasite's genome. The primers used for the
253 complementation of individual genes in the corresponding *Toxoplasma* knockout mutants and the
254 verification of their integration are listed in the **Supplementary Table 3.**
255
256 *(4) Generation of the ferrochelatase (TgFECH) knockdown strain using the tetracycline-controlled TET-*
257 *OFF system.* The TaTiΔ*ku80*Δ*hxg* strain carries the required genetic elements to suppress gene
258 expression in response to the treatment of anhydrotetracycline (ATc)[22], thereby being used as a parental
259 strain to knock down *TgFECH* gene. To help recognize and evaluate the expression repression of *TgFECH*,
260 we first endogenously tagged it with a 3xmyc epitope C-terminally as described above to create a
261 TaTiΔ*ku80*::*TgFECH-3xmyc* strain. A 1kb region upstream the start codon of *TgFECH* was recognized as
262 the promoter region for a replacement with a tetracycline-responsive T7S4 promoter. To achieve this, the
263 50-bp regions upstream and downstream the *TgFECH* promoter region were incorporated at the 5'- and
264 3'-ends of the pyrimethamine resistance cassette and a tetracycline-responsive T7S4 promoter by PCR
265 using a similar strategy as mentioned above. A single clone of TaTiΔ*ku80*::*TgFECH-3xmyc* was
266 transfected with the T7S4 promoter-encoding PCR product along with a guide RNA expression construct
267 recognizing the 5'-end of *TgFECH* gene to create a T7S4-TgFECH-3xmyc strain. Please refer to **Fig. S3a**
268 for the schematic description of the detailed steps. The epitope tag integration and the promoter
269 replacement were confirmed by PCR (**Fig. S3b**). The primers used for the generation of the *TgFECH*
270 knockdown strain and its verification are listed in the **Supplementary Table 3**.
271
272 (5) *Generation of nanoLuc luciferase (NLuc)-expressing parasite strains.* The *NLuc* expression plasmids
273 were transfected into individual Δ*cpox* and Δ*ppo* parasite strains and the corresponding Δ*cpoxCPOX* and
274 Δ*ppoPPO* complementation strains. The resulting *NLuc*-expressing strains were drug-selected and cloned
275 out. Individual clones for each strain were screened by their luciferase activities to help select clones

276 expressing similar levels of NLuc activities. These clones were maintained for downstream assays on
277 intracellular growth and IC_{50} determination for PPO inhibitors.
278
279 **SDS-PAGE and immunoblotting**
280 *Toxoplasma* parasites were grown and maintained in HFFs for a routine 2-day pass. Filter-purified
281 parasites were resuspended in 1x SDS-PAGE sample buffer (40 mM Tris, pH 6.8, 1% SDS, 5% glycerol,
282 0.0003% bromophenol blue, 50 mM DTT) and boiled for 10 min prior to resolving on SDS-PAGE.
283 Separated polypeptides were transferred to PVDF membranes via semi-dry protein transfer. For
284 chemiluminescence-based detection, blots were blocked with 5% non-fat milk, incubated with primary
285 antibody diluted in 1% non-fat milk in PBS, followed by probing with goat anti-mouse or anti-rabbit IgG
286 antibodies conjugated with horseradish peroxidase as the secondary antibody diluted in 1% non-fat milk
287 in PBS. Immunoblots were developed with SuperSignal WestPico chemiluminescent substrate (Thermo).
288 For fluorescence-based detection, blots were blocked with 1.25% fish gelatin in 500 mM Tris, pH 7.4, 1.5
289 M NaCl, incubated with primary antibody diluted in wash buffer (0.1% Tween-20 in PBS), followed by
290 probing with goat anti-mouse or anti-rabbit IgG antibodies conjugated with 680RD or 800CW dyes as the
291 secondary antibody (LI-COR). The chemiluminescence and fluorescence signals were captured using the
292 Azure C600 Imaging System.
293
294 **Immunofluorescence microscopy**
295 Freshly lysed parasites were used to infect confluent HFF cells pre-seeded in an 8-well chamber slide for
296 1 h (pulse-invaded parasites) or 18-24 h (replicated parasites). Immunofluorescence was performed as
297 described previously[20]. Images were viewed, digitally captured using a Leica CCD camera equipped with
298 a Leica DMi8 inverted epifluorescence microscope, and processed with Leica LAS X software.
299
300 **PPIX-based total heme quantification**
301 The parasites were grown in HFFs for 2 days in regular D10 medium or the medium supplemented with
302 chemicals indicated in the text before harvest. Freshly lysed parasites were syringed, filter-purified, and

303 washed in ice-cold PBS buffer. The parasites were finally resuspended in 400µl of ice-cold PBS buffer,
304 and sonicated on ice using a Branson analog sonifier with a mini horn at the output intensity setting of 3
305 and duty% of 20% at a 10-sec interval for 4 times. A thirty-second rest was set between each sonication
306 to avoid overheating. One hundred microliters of samples were mixed with 900 µl of 2 M oxalic acid in solid
307 black Eppendorf tubes and boiled for 30 min. Similarly, each sample was duplicated in the same way
308 without boiling, serving as a background. The heme solutions at 0, 5, 14.7, 44.3, 133, 400, and 1200 nM
309 were included in the assay to produce a standard curve. The fluorescence was recorded at 400 nm
310 excitation wavelength and 608 nm emission wavelength by BioTek H1 Hybrid plate reader. The
311 fluorescence of non-boiled samples will be subtracted from that of boiled samples. The final fluorescence
312 was normalized against the amount of parasite for comparison. The normalized heme abundance in WT
313 parasites was set at 100% to calculate the relative heme abundance in other strains.
314
315 **Plaque assay of *T. gondii***
316 Freshly egressed parasites were filter-purified and resuspended in D10 medium. Two hundred parasites
317 were inoculated into a 6-well plate seeded with confluent HFFs. The plate was incubated at 37ºC with 5%
318 CO_2 for 7 days without disturbance. The developed plaques were stained with 0.002% crystal violet in 70%
319 ethanol for 5 min and washed with water to enhance visualization of developed plaques. The plaques were
320 scanned to capture the images of entire wells or observed under a microscope under 25x magnification by
321 Leica DMi8 microscope. At least 50 individual plaques were photographed to measure their sizes. The
322 plaque size was plotted for comparison.
323
324 **Replication assay of *T. gondii***
325 For the parasite replication assay, freshly lysed parasites were filter-purified and inoculated into individual
326 wells of an 8-well chamber slide pre-seeded with HFF cells at approximately 1 x 10^5 cells per well and
327 incubated at 37ºC with 5% CO_2. Non-invaded parasites were washed off at 4 h post-infection. Invaded
328 parasites were allowed to infect host cells for an additional 24 and 36 h before fixation. The infected host
329 cells were stained with monoclonal anti-TgGRA7 (1:2,000) antibody and DAPI to help distinguish individual

330 parasitophorous vacuoles (PVs) and parasite nuclei, respectively. Slides were subjected to standard
331 immunofluorescence microscopy for imaging. One hundred PVs were enumerated for each strain and
332 plotted as average parasites per PV for comparison.
333
334 **Bioluminescence-based growth assay**
335 Individual strains were purified, resuspended in D10 medium, and inoculated into 96-well plate pre-seeded
336 with confluent HFFs. Parasites were allowed to invade host cells for 4 h at 37ºC with 5% CO_2 before
337 washing away non-invaded parasites, and the bioluminescence of invaded parasites at 4 h post-infection
338 was measured for normalization. Invaded parasites incubated at 37ºC with 5% CO_2 for an additional 96 h,
339 and their bioluminescence was measured every 24 h and normalized against the signal derived at 4 h for
340 the calculation of the fold change of bioluminescence, which reflects parasite intracellular growth rate.
341
342 **Mouse studies**
343 Six- to eight-week-old, outbred CD-1 mice were infected with WT or transgenic parasite strains diluted in
344 PBS with inocula indicated in the text by subcutaneous injection. The infected mice were monitored daily
345 for developing symptoms over 30 days. Mice that appeared moribund were humanely euthanized via CO_2
346 overdose, in compliance with the protocol approved by Clemson University's Institutional Animal Care and
347 Use Committee (Animal Welfare Assurance A3737-01, protocol number AUP2016-012). The
348 seroconversion of the surviving mice was tested by enzyme-linked immunosorbent assay (ELISA). The
349 surviving mice were allowed to rest for 10 days, prior to subcutaneous challenge injection with 1000 WT
350 parasites, and were kept for daily monitoring of survival for an additional 30 days. The mice survival curve
351 was plotted for statistical significance calculation by using the Log-rank (Mantel-Cox) test.
352
353 **Yeast complementation assay**
354 To test the functionality of the *Toxoplasma* orthologs of the heme biosynthetic proteins, we complemented
355 these orthologs in the corresponding yeast knockouts. First, we PCR-amplified the G418 resistance
356 cassette from the plasmid pFA6a-6xGLY-Myc-kanMX6 (Addgene, plasmid #:20769), flanked by 50-bp

357 upstream and downstream regions of the start and stop codons of the corresponding heme biosynthetic
358 gene, respectively. Approximately 5 μg of PCR products were transformed into the haploid yeast strain
359 BY4741 (GE Healthcare Dharmacon Inc., catalog number: YSC 1048) to remove the coding sequences of
360 heme biosynthetic genes by homologous recombination by using standard yeast transformation
361 procedures (**Fig. S6a**). The transformants were selected on YPD plate containing 200 μg/ml of G418 and
362 15 μg/ml hemin. After two to three days of incubation, the correct yeast knockouts were identified by PCR
363 (**Fig. S6b**). Next, we amplified the coding sequences of the corresponding *Toxoplasma* orthologs of
364 individual heme biosynthetic genes from *Toxoplasma* cDNA library by PCR and drove its expression under
365 the promoter of the yeast TEF1 gene in the pXP318 yeast expression construct to create a
366 complementation construct. The yeast complementation construct was chemically introduced into the
367 corresponding yeast knockout. The pXP318 encodes an uracil biosynthesis gene, while the WT yeast
368 strain shows an uracil auxotrophy phenotype. Therefore, the successful transformants receiving pXP318
369 or pXP318-derived plasmids did not require the addition of uracil in the growth medium. The yeast knockout
370 complemented with the corresponding *Toxoplasma* orthologs were also patched onto the plate lacking
371 exogenously added heme to evaluate its heme autotrophy phenotype. The primers used for the yeast
372 knockout generation and complementation of individual *Toxoplasma* orthologs are listed in the
373 **Supplementary Table 3**.
374
375 **Synthesis of oxadiazon derivatives**
376 All reagents were purchased from commercial sources and used without purification. ^{1}H and ^{13}C NMR
377 spectra were collected on Bruker 300 MHz NMR spectrometers using $CDCl_3$ as solvent. Chemical shifts
378 are reported in parts per million (ppm). Spectra are referenced to residual solvent peaks. Infrared
379 spectroscopy data were collected using an IR Affinity-1S instrument (with MIRacle 10 single reflection ATR
380 accessory). Flash silica gel (40–63 μm) was used for column chromatography. The compounds were
381 characterized by ^{1}H and ^{13}C NMR, ATR-FTIR, and HRMS. HRMS data were collected using an instrument
382 equipped with electrospray ionization in positive mode (ESI+) and a Time Of Flight (TOF) detector (**Fig.
383 S12 and S13**).

384

385 General Procedure for Oxadiargyl-triazole analogs[23]: Oxadiargyl (50 mg, 0.145 mmol, 1.0 equiv) was
386 dissolved in DCM/H_2O, 1:1 (0.5 mL) in a 20 mL round-bottomed flask equipped with a stir bar. The
387 appropriate azide (0.175 mmol, 1.2 equiv) was added, followed by anhydrous $CuSO_4$ (1 mg, 0.007 mmol,
388 0.05 equiv) and sodium ascorbate (4 mg, 0.02 mmol, 0.15 equiv). The resulting solution was then stirred
389 vigorously at rt for 4 h. The reaction was diluted with DCM (5 mL) and water (5 mL). The organic layer was
390 washed with saturated aq. brine, dried over anhydrous sodium sulfate, and concentrated by rotary
391 evaporation to provide the crude product as a brown oil. The isolate was purified by silica gel flash column
392 chromatography under the following gradient: hexanes (20 mL), ethyl acetate/hexanes (95:5; 20 mL), ethyl
393 acetate/hexanes (90:10; 50 mL), ethyl acetate/hexanes (80:20; 50 mL), ethyl acetate/hexanes (70:30; 50
394 mL), ethyl acetate/hexanes (50:50; 50 mL) to afford an opaque oil (62–87% isolated yield).

395

396 3-(5-((1-benzyl-*1H*-1,2,3-triazol-4-yl)methoxy)-2,4-dichlorophenyl)-5-(*tert*-butyl)-1,3,4-oxadiazol-2(*3H*)-
397 one (**Compound 1**):

398 Compound 1 was obtained in 62% yield using benzyl azide[24] (23 mg, 0.18 mmol, 1.2 equiv) as the azide
399 reagent.

400 Opaque oil; Yield: 62% (69 mg); R_f 0.54 (1:1 ethyl acetate/hexanes, UV); IR: (film) □ = 2970, 2924, 2856,
401 2094, 1782, 1489, 1246, 752, 717 cm^{-1}; ^1H NMR: (300 MHz, $CDCl_3$) δ 1.39 (s, 9H), δ 5.29 (s, 2H), δ 5.55
402 (s, 2H), δ 7.24 (s, 1H), δ 7.30 (m, 2H), δ = 7.38 (m, 2H), δ 7.52 (s, 1H), δ 7.61 (s, 1H); $^{13}C\{^1H\}$ NMR: (75
403 MHz, $CDCl_3$) δ = 27.0, 32.9, 54.3, 63.7, 113.8, 123.0, 123.9, 125.2, 128.1, 128.9, 129.2, 131.4, 134.3,
404 142.6, 152.0, 152.9, 163.6; HRMS (ESI-TOF): Calcd. for $C_{22}H_{22}Cl_2N_5O_3$, $[M+H]^+$ 474.1100 found m/z
405 474.1099.

406

407 5-(*tert*-butyl)-3-(2,4-dichloro-5-((1-octyl-*1H*-1,2,3-triazol-4-yl)methoxy)phenyl)-1,3,4-oxadiazol-2(*3H*)-one
408 (**Compound 2**):

409 Compound 2 was obtained in 87% yield using octyl azide[25] (24 mg, 0.18 mmol, 1.2 equiv) as the azide
410 reagent.

411 Opaque oil; Yield 87% (72 mg); R_f 0.50 (1:1 ethyl acetate/hexanes, UV); IR: (film) □ = 2951, 2924, 2854,
412 1786, 1479, 1246, 1126, 1041, 733 cm^{-1}; ^1H NMR: (300 MHz, $CDCl_3$) δ = 0.87 (t, 3H, *J* = 7 Hz), 1.26 (m,
413 12H), 1.38 (s, 9H), 1.92 (p, 2H, *J* = 7 Hz), 4.36 (t, 2H, *J* = 7 Hz), 7.26 (s, 1H), 7.52 (s, 1H), 7.68 (s, 1H);
414 $^{13}C\{^1H\}$ NMR: (75 MHz, $CDCl_3$) δ = 27.0, 32.9, 54.3, 63.7, 113.8, 122.9, 123.9, 125.1, 131.4, 142.6, 152.0,
415 152.9, 163.6; HRMS (ESI+-TOF): Calcd for $C_{23}H_{31}Cl_2N_5O_3$, $[M+H]^+$ 496.1882 Found m/z 496.1878.
416

417 ***In vitro* measurement of IC_{50}s for chemical inhibitors**

418 General procedures: Individual parasite strains expressing NanoLuc luciferase were used to infect
419 confluent HFFs pre-seeded into 96-well solid white plate with inocula of 1000 tachyzoites per well for
420 WT::*NLuc* and Δ*ppoPPO*::*NLuc* strains and 3000 tachyzoites per well for Δ*ppo*::*NLuc* strain. Higher
421 inoculum of Δ*ppo*::*NLuc* were adjusted in the assay to help accurately quantify fold change of luciferase
422 activity due to its slow growth. Purified parasites were resuspended in phenol red free D10 medium, and
423 150 µl of parasite resuspension for individual strains were inoculated each well. Parasites were initially
424 incubated at 37ºC with 5% CO_2 for 4 h to facilitate host invasion. Next, the media were gently aspirated
425 and switched to the phenol red free D10 media containing individual chemical inhibitors at the serial
426 concentrations listed below. A control medium without an inhibitor was included for luciferase activity
427 normalization. After 2- to 4-day incubation with chemical inhibitors, the media were gently aspirated to
428 avoid disturbance of monolayer HFFs, changed to the 12.5 µM Coelenterazine h in lysis buffer (100 mM
429 4-Morpholineethanesulfonic acid (MES) pH 6.0, 1 mM trans-1,2-Diaminocyclohexane-N,N,N′,N′-tetraacetic
430 acid (CDTA), 0.5% (v/v) Tergitol, 0.05% (v/v) Mazu DF 204, 150 mM KCl, 1 mM DTT, and 35 mM thiourea),
431 and incubated at room temperature for 10 min to fully lyse cells prior to luciferase activity quantification.
432 The signals under individual concentrations of inhibitors were recorded by BioTek plate reader and
433 normalized against the luciferase activities derived from the infected cells incubated in the plain medium.
434 The normalized luciferase activities were plotted against the concentrations of inhibitors to calculate the
435 IC_{50} values for individual inhibitors by the built-in "Dose-response-inhibition" program in GraphPad Prism
436 software (8th version).
437

438 *Measurement of IC_{50}s for the PPO inhibitors*

439 The serial concentrations of PPO inhibitors were 500.0, 125.0, 31.3, 7.81, 1.95, 0.488, 0.122, 3.05×10^{-2},
440 and 7.63×10^{-3} μM. The efficacies of these inhibitors were only tested on WT::*NLuc* parasites after 4 days
441 of growth.

442

443 *Measurement of IC_{50}s for Oxadiazon and its derivatives*

444 The serial concentrations of the chemicals were 500.0, 166.7, 55.6, 18.5, 6.17, 2.06, 6.8×10^{-1}, 2.3×10^{-1},
445 7.6×10^{-2}, 2.5×10^{-2}, and 8.5×10^{-3} μM. The efficacies of these inhibitors were tested on WT::*NLuc*,
446 Δ*ppo*::*NLuc*, and Δ*ppoPPO*::*NLuc* parasites after 4 days of growth.

447

448 *Measurement of IC_{50} for pyrimethamine*

449 The serial concentrations of pyrimethamine included in the media were 100.0, 33.3. 11.1, 3.70, 1.23, 0.41,
450 0.14. 0.045, 0.015, 5.1×10^{-3}, and 1.7×10^{-3} μM. The efficacy of pyrimethamine was tested on WT::*NLuc*,
451 Δ*ppo*::*NLuc*, and Δ*ppoPPO*::*NLuc* parasites after 4 days of growth.

452

453 *Measurement of IC_{50} for succinylacetone*

454 The serial concentrations of pyrimethamine included in the media were 100.0, 33.3. 11.1, 3.70, 1.23, 0.41,
455 0.14. 0.045, 0.015, 5.1×10^{-3}, and 1.7×10^{-3} μM. The IC_{50} value of succinylacetone was determined on its
456 inhibition on 2-day growth of WT::*NLuc* parasites.

457

458 **Resazurin-based cell viability assay**

459 The HFFs were seeded in 96-well plates and grown in regular D10 medium. After the host cells became
460 confluent, they were incubated in the media containing the tested PPO inhibitors in the serial
461 concentrations at 500.0, 166.7, 55.6, 18.5, 6.17, 2.06, 6.8×10^{-1}, 2.3×10^{-1}, 7.6×10^{-2}, 2.5×10^{-2}, and 8.5×10^{-3}
462 μM, or the media containing Triton X-100 at 1070.0, 356.7, 118.9, 39.6, 13.2, 4.40, 1.47, 0.49, 0.16, 0.054,
463 and 0.018 μg/ml. The host cells grown in regular D10 medium were included as the control for
464 normalization. The resazurin was diluted at 0.004% in regular D10 medium and incubated with host cells

465 at 37ºC with 5% CO_2 for 4 h before absorbance measurement at 570 and 600 nm by BioTek H1 Hybrid
466 plate reader. A resazurin-containing medium control without incubation with host cells was included to
467 calculate the absorbance ratio of oxidized resazurin at 570 nm vs. 600 nm, termed $OD(blank)_{570/600}$. The
468 normalized cell viability was calculated using the following equation: $[OD(inhibitor)_{570} - OD(inhibitor)_{600} \times$
469 $OD(blank)_{570/600}]/ [OD(medium)_{570} - OD(medium)_{600} \times OD(blank)_{570/600}] *100\%$.
470

471 **Phylogenetic tree construction**

472 Polypeptide sequences of 17 PPO orthologs from animals, plants, bacteria, protozoa, and fungi were
473 retrieved from the Uniport database (www.uniprot.org). The sequences were aligned using the CLUSTAL
474 MUSCLE (MUltiple Sequence Comparison by Log-Expectation) alignment tools[26,27]. The resulting
475 sequence alignment was used to construct a phylogenetic tree by using the Neighbor-Joining tree
476 analysis[28] built in the Geneious software. Bootstrap values based on 10,000 replicates are shown. The
477 sequences used for MUSCLE alignment were listed in **Fig. S8**.
478

479 **Statistical significance calculation**

480 The statistical significance calculation in this study was performed using GraphPad Prism software (8th
481 version). The methods for individual assays were indicated in the figure captions.
482

483 **Data availability.**

484 The data that support the findings of this study are available from the corresponding authors upon request.
485
486
487

Acknowledgements We thank our colleagues, Drs. Vern Carruthers, David Sibley, and Peter Bradley for sharing key reagents for this work. We also want to thank Drs. Vern Carruthers, James Morris, and Meredith Morris for critically reading this manuscript before submission. This work was supported by the Clemson Startup fund (to Z.D.), Knights Templar Eye Foundation Pediatric Ophthalmology Career-Starter Research Grant (to Z.D.), a pilot grant of an NIH COBRE grant P20GM109094 (to Z.D.), NIH R01AI111962 and R01AI056312 (to I.H.). The funders had no role in study design, data collection and analysis, decision to publish, or preparation of the manuscript.

Author contributions Z.D. designed this study. A.B., K.F., M.K., C.D, K.C.R., and Z.D. executed experiments. A.B., K.F., and Z.D. performed endogenous gene tagging and determined their subcellular locations by immunofluorescence microscopy and their expression in acute *Toxoplasma* infection via immunoblotting. A.B., K.F., C.D., and Z.D generated complete knockout or knockdown parasite strains and the corresponding complementation strains if needed. A.B., K.F., M.K., C.D., and Z.D. measured the replication, growth, and acute virulence for the heme-deficient parasites. A.B., K.F., and C.D. conducted plaque assays for the heme-deficient parasites. Z.D. generated the heme-deficient yeast strains and trans-complemented them with the corresponding wildtype *Toxoplasma* orthologs. A.B., K.F., M.K., and Z.D quantified heme abundances in the heme-deficient and drug-treated parasites. K.F. and Z.D. evaluated the inhibition efficacies of the PPO-targeting herbicides and their derivatives. K.C.R. and D.C.W. designed the strategy for chemical synthesis of oxadiazon derivatives and conducted the chemical modification. I.Q. provided analytic methods for heme quantification and technical support to this study. Z.D. wrote the original draft. A.B., K.F., M.K., C.D., K.C.R., D.C.W., I.Q., and Z.D. reviewed and revised the manuscript.

Competing interests The authors declare no competing interests.

Materials & Correspondence Please send inquiries to Zhicheng Dou, zdou@clemson.edu

514 **References**

515 1. Dailey, H. A. *et al.* Prokaryotic Heme Biosynthesis: Multiple Pathways to a Common Essential Product.
516 *Microbiol Mol Biol R* **81,** e00048-16 (2017).
517

518 2. Kořený, L., Oborník, M. & Lukeš, J. Make It, Take It, or Leave It: Heme Metabolism of Parasites. *Plos*
519 *Pathog* **9,** e1003088 (2013).
520

521 3. Kim, K. & Weiss, L. M. *Toxoplasma gondii*: the model apicomplexan. *Int J Parasitol* **34,** 423 432
522 (2004).
523

524 4. Wu, B. Heme biosynthetic pathway in apicomplexan parasites. *PhD Dissertation, University of*
525 *Pennsylvania* (2006).
526

527 5. Jaffe, E. K. *et al.* Crystal structure of *Toxoplasma gondii* porphobilinogen synthase: insights on
528 octameric structure and porphobilinogen formation. *J Biol Chem* **286,** 15298 15307 (2011).
529

530 6. Shanmugam, D., Wu, B., Ramirez, U., Jaffe, E. K. & Roos, D. S. Plastid-associated Porphobilinogen
531 Synthase from *Toxoplasma gondii* KINETIC AND STRUCTURAL PROPERTIES VALIDATE
532 THERAPEUTIC POTENTIAL. *J Biol Chem* **285,** 22122–22131 (2010).
533

534 7. Blader, I. J., Coleman, B. I., Chen, C.-T. & Gubbels, M.-J. Lytic Cycle of *Toxoplasma gondii*: 15 Years
535 Later. *Annu Rev Microbiol* **69,** 1–23 (2014).
536

537 8. Schwab, J., Beckers, C. & Joiner, K. The parasitophorous vacuole membrane surrounding intracellular
538 *Toxoplasma gondii* functions as a molecular sieve. *Proceedings of the National Academy of Sciences of*
539 *the United States of America* **91,** 509 513 (1994).
540

541 9. Gold, D. A. *et al.* The *Toxoplasma* Dense Granule Proteins GRA17 and GRA23 Mediate the
542 Movement of Small Molecules between the Host and the Parasitophorous Vacuole. *Cell Host Microbe*
543 **17,** 642 652 (2015).
544
545 10. Dou, Z., McGovern, O. L., Cristina, M. & Carruthers, V. B. *Toxoplasma gondii* Ingests and Digests
546 Host Cytosolic Proteins. *Mbio* **5,** e01188-14 (2014).
547
548 11. Sigala, P. A., Crowley, J. R., Henderson, J. P. & Goldberg, D. E. Deconvoluting heme biosynthesis to
549 target blood-stage malaria parasites. *Elife* **4,** 50 (2015).
550
551 12. Nagaraj, V. *et al.* Malaria parasite-synthesized heme is essential in the mosquito and liver stages and
552 complements host heme in the blood stages of infection. *Plos Pathog* **9,** e1003522 (2013).
553
554 13. Ke, H. *et al.* The heme biosynthesis pathway is essential for *Plasmodium falciparum* development in
555 mosquito stage but not in blood stages. *J Biol Chem* **289,** 34827 34837 (2014).
556
557 14. Giaever, G. *et al.* Functional profiling of the *Saccharomyces cerevisiae* genome. *Nature* **418,** 387 391
558 (2002).
559
560 15. Fan, T., Grimm, B. & Layer, G. Porphyrin and heme synthesis. *Adv Bot Res* 89–131 (2019).
561 doi:10.1016/bs.abr.2019.06.001
562
563 16. Tanaka, A. & Tanaka, R. Chlorophyll metabolism. *Curr Opin Plant Biol* **9,** 248–255 (2006).
564
565 17. Duke, S. O. *et al.* Protoporphyrinogen Oxidase-Inhibiting Herbicides. *Weed Sci* **39,** 465–473 (1991).
566
567 18. Hooda, J., Shah, A. & Zhang, L. Heme, an essential nutrient from dietary proteins, critically impacts

568 diverse physiological and pathological processes. *Nutrients* **6,** 1080 1102 (2014).
569
570 19. Khan, A. A. & Quigley, J. G. Control of intracellular heme levels: Heme transporters and heme
571 oxygenases. *Biochimica Et Biophysica Acta Bba - Mol Cell Res* **1813,** 668 682 (2011).
572
573 20. Thornton, B. L. *et al.* An ortholog of *Plasmodium falciparum* chloroquine resistance transporter
574 (PfCRT) plays a key role in maintaining the integrity of the endolysosomal system in *Toxoplasma gondii*
575 to facilitate host invasion. *Plos Pathog* **15,** e1007775 (2019).
576
577 21. Shen, B., Brown, K. M., Lee, T. D. & Sibley, D. L. Efficient Gene Disruption in Diverse Strains of
578 *Toxoplasma gondii* Using CRISPR/CAS9. *Mbio* **5,** e01114-14 (2014).
579
580 22. Sheiner, L. *et al.* A systematic screen to discover and analyze apicoplast proteins identifies a
581 conserved and essential protein import factor. *Plos Pathog* **7,** e1002392 (2011).
582
583 23. Liang, L. & Astruc, D. The copper(I)-catalyzed alkyne-azide cycloaddition (CuAAC) “click” reaction
584 and its applications. An overview. *Coordin Chem Rev* **255,** 2933–2945 (2011).
585
586 24. Bahsis, L. *et al.* A reusable polymer-supported copper(I) catalyst for triazole click reaction on water:
587 An experimental and computational study. *Appl Organomet Chem* **33,** e4669 (2019).
588
589 25. Yang, C., Flynn, J. P. & Niu, J. Facile Synthesis of Sequence-Regulated Synthetic Polymers Using
590 Orthogonal SuFEx and CuAAC Click Reactions. *Angewandte Chemie Int Ed* **57,** 16194–16199 (2018).
591
592 26. Edgar, R. C. MUSCLE: a multiple sequence alignment method with reduced time and space
593 complexity. *Bmc Bioinformatics* **5,** 113 (2004).
594

595 27. Edgar, R. C. MUSCLE: multiple sequence alignment with high accuracy and high throughput. *Nucleic*
596 *Acids Res* **32,** 1792–1797 (2004).
597
598 28. Saitou, N. & Nei, M. The neighbor-joining method: a new method for reconstructing phylogenetic
599 trees. *Mol Biol Evol* **4,** 406–25 (1987).
600

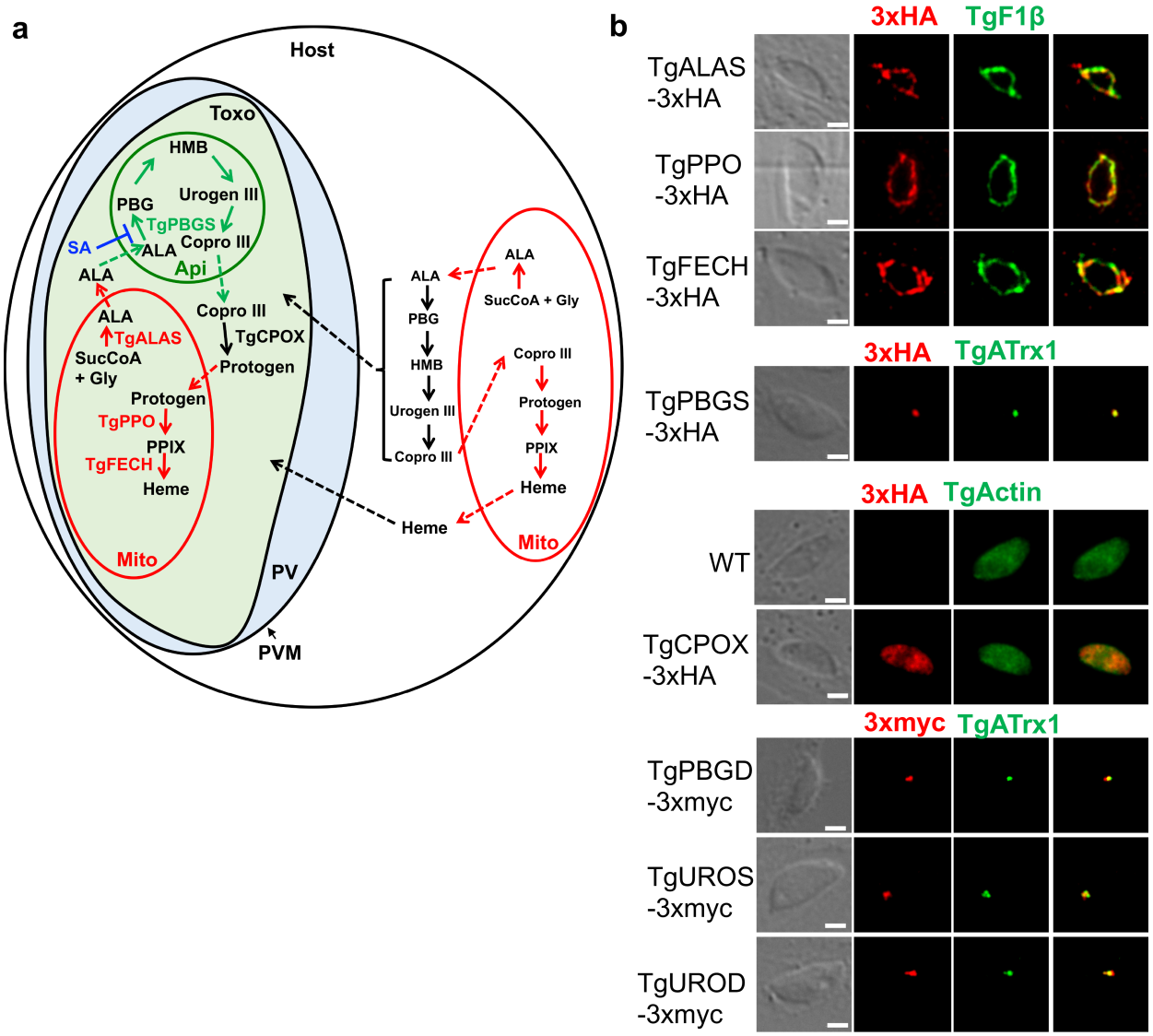

Fig. 1 | *Toxoplasma gondii* encodes its *de novo* heme biosynthetic pathway within 3 subcellular locations. a, The working model of the *de novo* heme biosynthesis in *Toxoplasma* parasites. The enzymes catalyzing the *de novo* heme biosynthesis are distributed within three subcellular locations in the parasites, whereas they are only localized in the mitochondria and cytoplasm in mammals. **b,** Determination of the expression of the heme biosynthetic genes in *Toxoplasma* during its acute infection and their subcellular locations by endogenous gene tagging with 3xHA or 3xmyc epitopes. A subunit of *Toxoplasma* mitochondrial ATPase (TgF1β) and an apicoplast-associated thioredoxin family protein (TgATrx1) were used as the mitochondria and apicoplast markers, respectively. TgActin was used as a cytoplasm marker. Bar = 2 μm. ALA, Aminolevulinic acid; ALAS, Aminolevulinic acid synthase; Api, apicoplast; Copro III, coproporphyrinogen III; CPOX, Coproporphyrinogen III oxidase; FECH, Ferrochelatase; Gly, glycine; HMB, hydroxymethylbilan; IVN, intravacuolar network; Mito, mitochondria; PBG, porphobilinogen; PBGD, Porphobilinogen deaminase; PBGS, Porphobilinogen synthase; PPIX, protoporphyrin IX; PPO, Protoporphyrinogen oxidase; Protogen, protoporphyrinogen IX; PV, parasitophorous vacuole; PVM, parasitophorous vacuole membrane; SucCoA, Succinyl-CoA; Toxo, *Toxoplasma gondii*; UROD, Uroporphyrinogen III decarboxylase; Urogen III, uroporphyrinogen III; UROS, Uroporphyrinogen III Synthase.

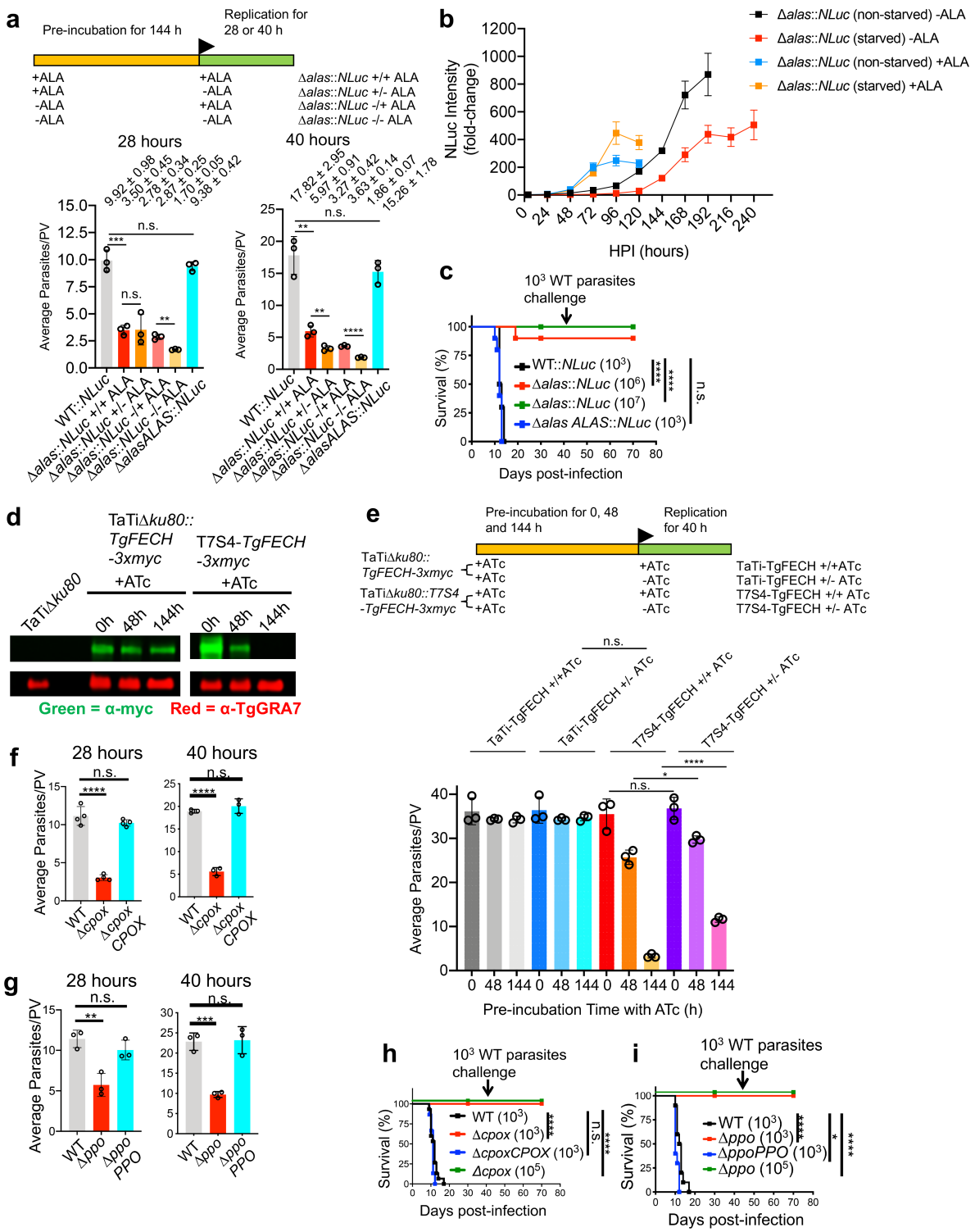

Fig. 2 | *Toxoplasma* parasites principally rely on their *de novo* heme biosynthesis for intracellular growth and pathogenesis. a, Replication comparison of the starved and non-starved Δ*alas*::*NLuc* parasites in the media containing or lacking ALA. Data represent mean ± SD of n=3 biological replicates. **b,** A 10-day growth assay of the starved and non-starved Δ*alas*::*NLuc* parasites in ALA-containing or deficient media. Error bars represent SEM of n=3 biological replicates with 3 technical replicates each. **c,** Acute virulence determination of *TgALAS*-deficient parasites in a murine model. Ten mice of equal numbers of males and females were used for each strain. **d,** Evaluation of repression efficiency of TgFECH by ATc treatment via immunoblotting. *TgFECH* was endogenously tagged with a 3xmyc tag at its C-terminus for recognition by immunoblotting. The lysates were also probed against TgGRA7 as loading control. **e,** Replication assessment of the *TgFECH* knockdown parasites. T7S4-TgFECH and its parental strains were pre-treated with ATc for the period described in the scheme before replication assay. Data represent mean ± SD of n=3 biological replicates. **f-g,** Replication assay of Δ*cpox* and Δ*ppo* parasites. Data represent mean ± SD of n=3-4 biological replicates. **h-i,** Acute virulence measurement of Δ*cpox* and Δ*ppo* parasites in a murine model. 5 male and 5 female mice were used for each strain. Statistical significance of the animal studies in **c, h,** and **i** was calculated using the Log-rank (Mantel-Cox) test. Statistical significance in the rest of the studies was calculated by two-tailed unpaired Student's *t*-test. *, $p<0.05$; **, $p<0.01$; ***, $p<0.001$; ****, $p<0.0001$; n.s., not significant.

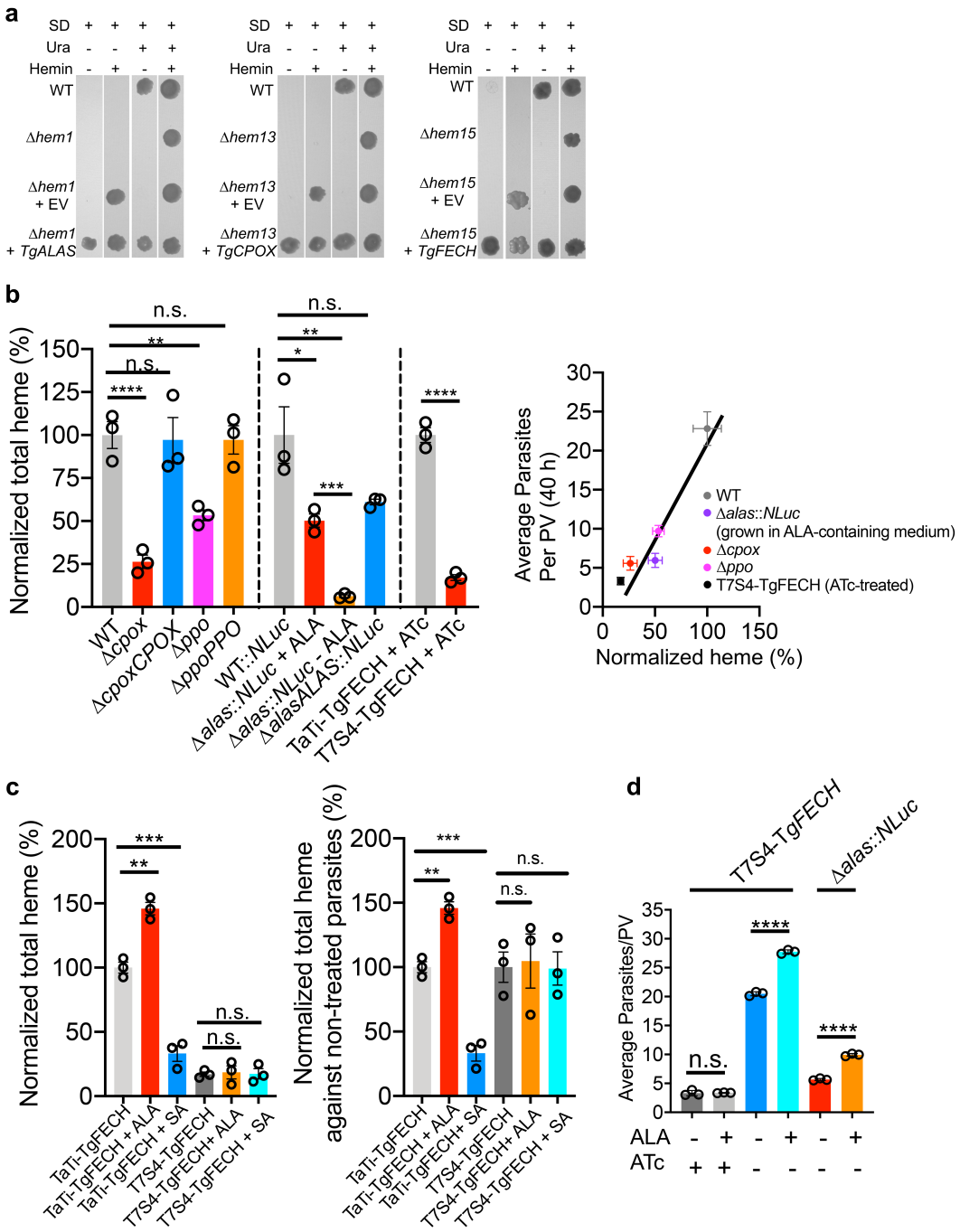

Fig. 3 | *Toxoplasma* harbors an active *de novo* heme biosynthetic pathway. a, Complementation of *Toxoplasma* orthologs of heme biosynthetic genes in the corresponding *S. cerevisiae* heme-deficient knockouts. EV, empty vector; SD, synthetic defined medium; Ura, uracil. **b,** Total heme quantification in heme-deficient parasites. A protoporphyrin IX-based fluorescence assay was used to quantify the total heme. The total heme levels in transgenic parasite strains were normalized against the corresponding parental strains. The average replication rates showed a positive correlation with the normalized heme abundances. Data represent mean ± SEM of n=3 biological replicates with 3 technical replicates each. **c,** Chemical interference in heme production in the parasites requires a functional heme biosynthetic pathway in *Toxoplasma*. The *TgFECH* knockdown parasites along with its parental strain were treated with ATc for 144 h before stimulation or repression of heme production by ALA or SA, respectively. Data represent mean ± SEM from n=3 biological replicates. **d,** Partial restoration of *TgFECH* expression in ATc-treated T7S4-TgFECH parasites helped them respond to the growth stimulation by ALA treatment. Data represent mean ± SD of n=3 biological replicates. Statistical significance in all of the studies listed in this figure was calculated by two-tailed unpaired Student's *t*-test. *, $p<0.05$; **, $p<0.01$; ***, $p<0.001$; ****, $p<0.0001$; n.s., not significant.

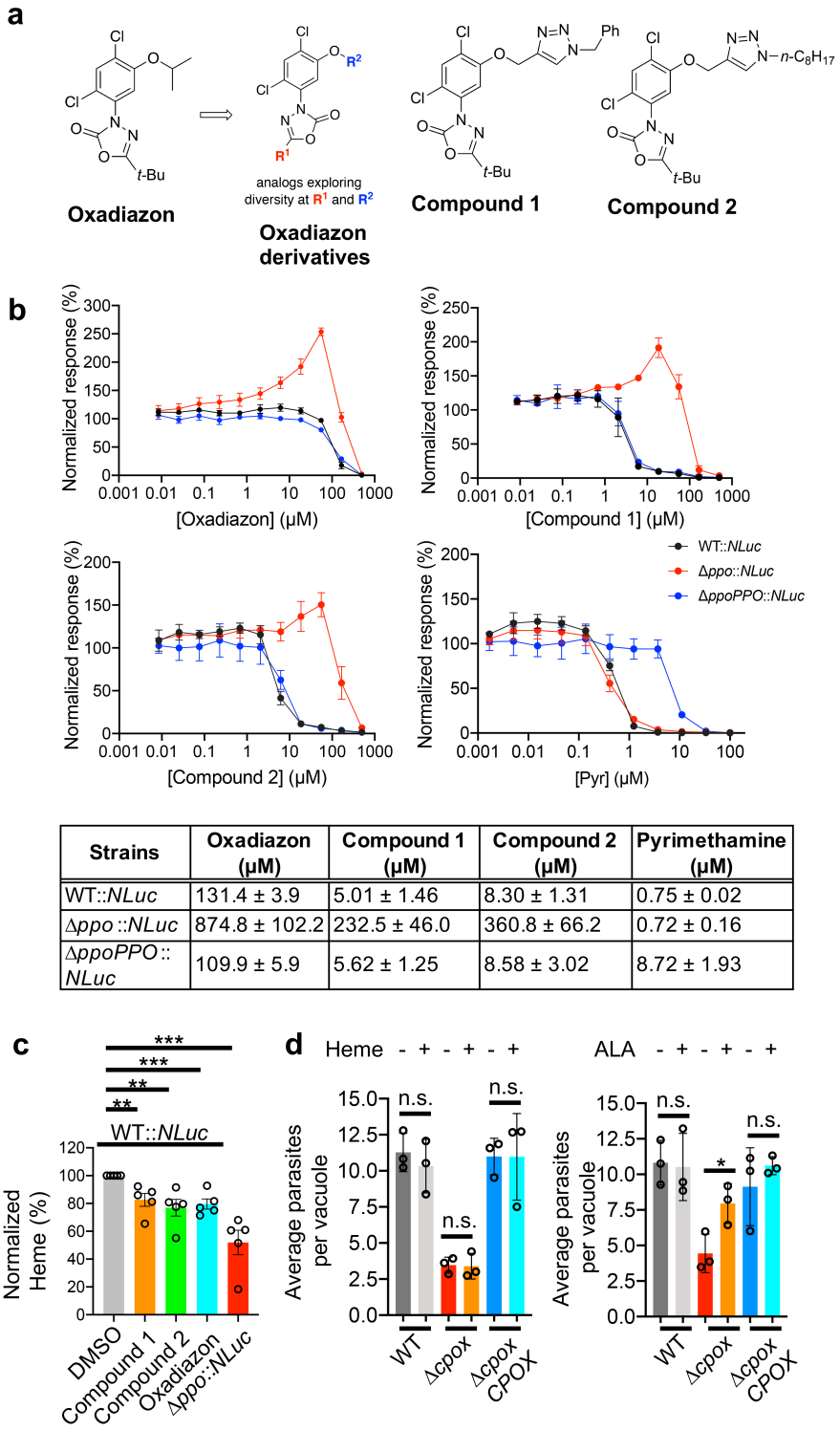

Strains	Oxadiazon (μM)	Compound 1 (μM)	Compound 2 (μM)	Pyrimethamine (μM)
WT::*NLuc*	131.4 ± 3.9	5.01 ± 1.46	8.30 ± 1.31	0.75 ± 0.02
Δ*ppo* ::*NLuc*	874.8 ± 102.2	232.5 ± 46.0	360.8 ± 66.2	0.72 ± 0.16
Δ*ppoPPO* :: *NLuc*	109.9 ± 5.9	5.62 ± 1.25	8.58 ± 3.02	8.72 ± 1.93

Fig. 4 | Chemical interrogation of the *Toxoplasma's de novo* heme production by oxadiazon and its derivatives reduces the intracellular growth of the parasites. a, Chemical structure of oxadiazon and two derivatives. **b,** Efficacy determination of oxadiazon and its derivatives in the inhibition of WT *Toxoplasma* growth by using a luciferase-based growth assay. The Δ*ppo*::*NLuc* and Δ*ppoPPO*::*NLuc* were included for evaluating the target specificity of the inhibitors to TgPPO. Pyrimethamine, an antibiotic targeting a folic acid metabolism that is irrelevant to heme biosynthesis, was also included for assessing the specificity of these PPO inhibitors. Data shown in the table represent mean ± SEM of n=3 biological replicates with 3 technical replicates each. **c,** Heme levels were reduced in the parasites upon treatment with oxadiazon and its derivatives. Data shown here represent mean ± SEM of n=5 biological replicates. **d,** *Toxoplasma* was incapable of taking up extracellular heme to support its intracellular growth. Data represent mean ± SD of n=3 biological replicates. Statistical significance for the assays described in this figure was determined by two-tailed unpaired Student's *t*-test. *, $p<0.05$; **, $p<0.01$; ***, $p<0.001$; n.s., not significant.